Reprinted from December 1982, Vol. 104, Journal of Fluids Engineering

C. E. Brennen

Professor of Mechanical Engineering.

C. Meissner

E. Y. Lo

G. S. Hoffman

Former Undergraduates.

California Institute of Technology, Pasadena, Calif. 91125

Scale Effects in the Dynamic Transfer Functions for Cavitating Inducers

Dynamic transfer functions for two cavitating inducers of the same geometry but different size are presented, compared, and discussed. The transfer functions for each inducer indicate similar trends as the cavitation number is decreased. The nondimensional results for the two sizes are compared with themselves and with theoretical calculations based on the Bubbly Flow Model (reference [2]). All three sets of results compare well and lend further credance to the theoretical model. The best values of the two parameters in the model (K and M) are evaluated and recommended for use in applications.

1 Introduction

The purpose of this paper is to present further data on the dynamic transfer functions for cavitating inducers. The earlier experiments of Ng and Brennen [1] presented measured transfer functions for a 7.6 cm diameter model of the low pressure oxidizer turbopump in the Space Shuttle Main Engine (SSME). In a later paper [2] a theoretical model of the unsteady cavitating flow in an inducer was presented which, despite many approximations, yielded transfer functions which exhibited many of the qualitative dynamic characteristics of the experimental measurements. For the purpose of more detailed quantitative rather than qualitative comparison, it was necessary to assume values for two scalar quantities which are crucial to the model. One of these (K in reference [2]) essentially represents the mean compressibility of the bubbly cavitating flow; the other (M in reference [2]) is the factor of proportionality between the fluctuating angle of attack at the inducer inlet and the fluctuating rate of production of cavitating bubbles in the neighborhood of inlet.

This paper presents further experimental measurements of transfer functions specifically for larger, 10.2 cm diameter inducers. A number of inducers were used but presentation here will be confined to the results for a 10.2 cm model of the SSME inducer. Comparison with the results for the geometrically similar 7.6 cm inducer allows some limited evaluation of the effects of scale on the transfer function elements (and on K and M). Furthermore, the more extensive data base and the improvement in the quality of the data permit a more critical examination of the theoretical "bubbly-flow" model and lead to a more definitive recommendation for the empirical constants K and M.

Like the previous experiments, the present results were obtained in the Dynamic Pump Test Facility which has been previously described in reference [1]. For the present experiments an alternative working section was constructed to accommodate 10.2 cm impellers. However, the same volute was used for both impeller sizes. Furthermore, new dynamic instrumentation was added in the form of electromagnetic meters to supplement the earlier measurements of fluctuating flow rate (see Fig. 1). As previously discussed (references [1] and [11]) the measurement of the fluctuating flow rates (2 to 4 percent of the mean flow rate) into and out of the pump are the most critical aspect of these kinds of experiments. As described in reference [11], the modified Foxboro electromagnetic meters (EMM) provided significant improvement in the dynamic data over that obtained with the laser doppler velocimeters (LDV). This was due primarily to the fact that the EM meters provide a true integrated measure of the instantaneous volume flow rate [3] in these unsteady flows. Such a measure is difficult to achieve with the point velocity measurements using the LDV, particularly in the presence of oscillating flow boundary layers. Some details on both the steady calibration of the EM meters and an in-line comparison of the dynamic performance of the EMM and LDV are included in reference [11].

2 Steady State Inducer Pump Performance

The difference in performance between the two geometrically similar inducers was investigated and found to be caused by differences in the efficiency of pressure recovery in the volute. The latter was not scaled up but merely modified at inlet to accommodate the 10.2 cm impellers. The resulting difference in the slope of the performance curves at a flow coefficient, $\phi = 0.07$ (for which dynamic transfer matrices were obtained) causes some difference in the "resistance" component (real part of Z_{12}) of the transfer matrices for the two impellers; further discussion on this is delayed until Section 5.

The cavitation performance of the 10.2 cm impeller is presented in Fig. 3. Comparison of this data with the

Contributed by the Fluids Engineering Division for publication in the JOURNAL OF FLUIDS ENGINEERING. Manuscript received by the Fluid Engineering Division, September 26, 1979.

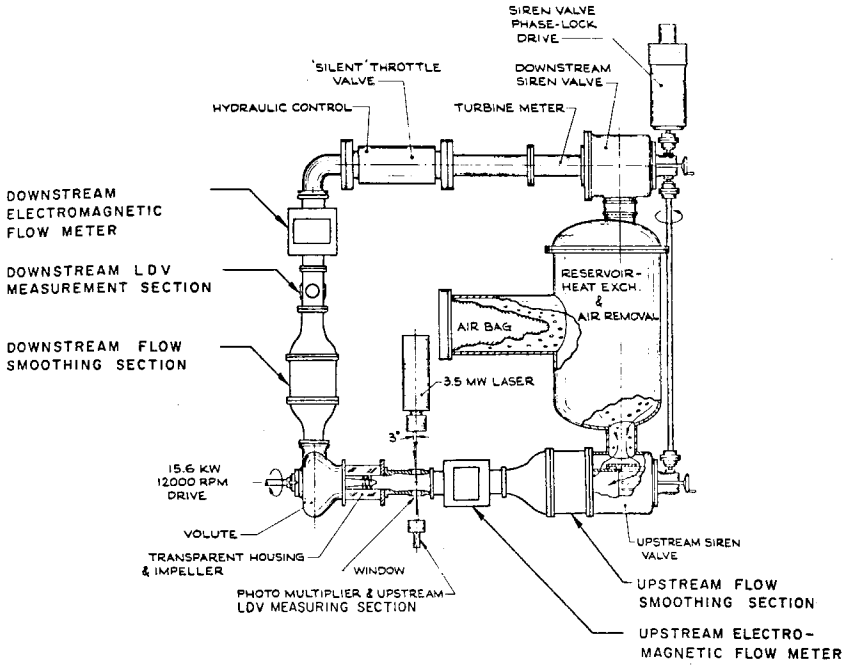

Fig. 1 Schematic plan view of the modified Dynamic Pump Test Facility

cavitation performance of the 7.6 cm impeller (see Fig. 4 of reference [1]) indicates that the curves are merely displaced vertically due to the differences in pressure recovery in the volute and that the essential nature of the cavitation effect is unchanged. Also shown in Fig. 3 are the mean flow conditions at which dynamic transfer matrices were obtained; these are identified by letters which will be used for identification in later figures.

Both steady state performance data and dynamic transfer functions were also obtained with various prerotation inhibiting devices installed several diameters upstream of the inducers. The effects of these devices are reported briefly in reference [11].

3 Dynamic Transfer Matrices

The dynamic transfer matrices reported here use the definition described previously ([1], [2])

$$\begin{Bmatrix} \tilde{h}_2 - \tilde{h}_1 \\ \tilde{m}_2 - \tilde{m}_1 \end{Bmatrix} = \begin{Bmatrix} ZP_{11} & ZP_{12} \\ ZP_{21} & ZP_{22} \end{Bmatrix} \begin{Bmatrix} \tilde{h}_1 \\ \tilde{m}_1 \end{Bmatrix}$$

where $\tilde{h}$, $\tilde{m}$ are nondimensional fluctuating total pressure and mass flow rate quantities which are complex in general. Subscripts 1 and 2 refer to inlet and discharge quantities. The transfer matrix $[ZP]$ is a complex function of the mean flow conditions (ϕ, σ) and the reduced frequency, ω.

The experimental and data reduction methods used to obtain $[ZP]$ matrices between the inducer inlet and the volute discharge were similar to those described by Ng and Brennen [1]. However, two differences should be noted. First, the addition of the electromagnetic flow meters allowed separate evaluation of transfer matrices using the simultaneous measurements from either the EM meters or the laser doppler velocimeters. Second, in order to accommodate the discharge EM meter, the downstream smoothing section between the volute discharge and the downstream LDV was considerably shortened and strengthened. This significantly reduced the corrections which were originally used by Ng and Brennen [1] to obtain the pump transfer matrix, $[ZP]$, from the overall measured $[Z]$ matrix. Furthermore, all the corrections described in that previous paper are smaller in relative magnitude for the 10.2 cm impellers than for the 7.6 cm impellers. The net result is a substantial improvement in accuracy over the transfer functions previously presented for the 7.6 cm impellers.

The presentation of the transfer functions is similar to that employed previously. The real and imaginary parts of the elements of $[ZP]$ are plotted as solid and dashed lines, respectively, in graphs against reduced frequency, ω. All of the transfer functions presented here for the 10.2 cm impeller

Nomenclature

a_{NIJ} = coefficients in the polynomial fits to the transfer matrices
A_i = inducer inlet area
F = blade passage frictional resistance parameter
h = inducer blade tip spacing
$\tilde{h}$ = nondimensional fluctuating total pressure, $\tilde{h}^*/1/2\rho U_T^2$
$\tilde{h}^*$ = fluctuating total pressure
I, J = dummy subscripts equal to 1 or 2
j = imaginary unit
K = parameter of bubbly flow model
M = parameter of bubbly flow model
$\tilde{m}$ = nondimensional fluctuating mass flow rate, $\tilde{m}^*/\rho U_T A_i$
$\tilde{m}^*$ = fluctuating mass flow rate
N = integer power and subscript
U_A = mean axial velocity at inducer inlet
U_T = inducer tip speed
ZP_{IJ} = inducer pump transfer matrix
γ = blade angle at inducer inlet tip
ϵ = fractional length of blade passage containing bubbly mixture
ϕ = flow coefficient, U_A/U_T
ψ = head coefficient, total pressure rise $\div \rho U_T^2$
ρ = water density
σ = cavitation number, inlet pressure minus vapor pressure $\div 1/2\,\rho U_T^2$
τ = ratio of inducer axial length to blade tip spacing
Ω = radian frequency of perturbations
ω = reduced frequency $\Omega h/U_T$

Subscripts 1 and 2 on $\tilde{h}$ and $\tilde{m}$ refer to the inlet and discharge quantities.

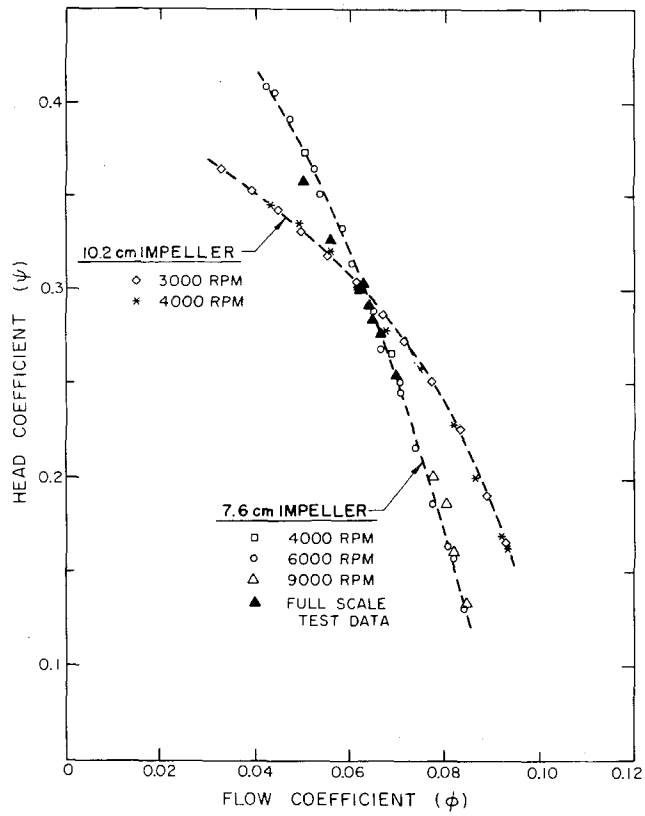

Fig. 2 Noncavitating performance of the 7.6 cm and 10.2 cm diameter models of the low pressure oxidizer inducer pump in the SSME at various rotating speeds. Also shown are some full scale data [4]. Uncertainties are about ±0.002 on the ordinate and ±0.001 on the abscissa.

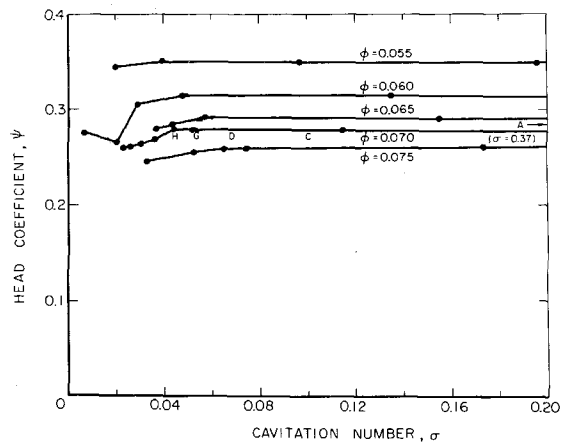

Fig. 3 Cavitation performance at the 10.2 cm diameter model at various flow coefficients taken with a uniform honeycomb in the inlet flow. The points at which transfer functions were obtained are indicated by the letters, A, C, D, G, and H. Uncertainties are about ±0.002 on the ordinate and abscissa.

were obtained from the EMM flow rate measurements, though simultaneous LDV transfer functions were also obtained in all cases. As discussed previously, the EMM transfer functions were believed to be superior; one comparison of EMM and LDV transfer functions is included in reference [11].

4 Comparison of the Transfer Matrices for the Two Sizes of Impeller

Figure 4 presents the measured transfer functions for the 10.2 cm impeller at $\phi = 0.07$ and various cavitation numbers. The latter range from $\sigma = 0.37$ for the point A at which there

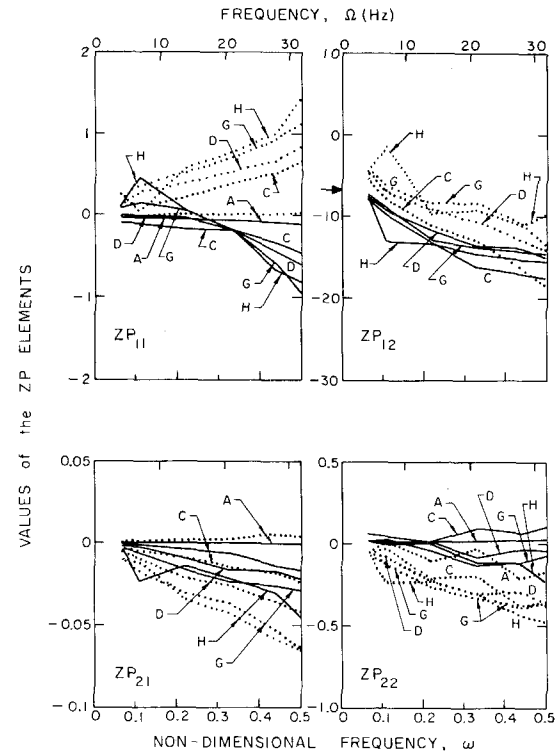

Fig. 4 Transfer matrices for the 10.2 cm impeller at $\phi = 0.07$, a rotating speed of 6000 rpm and various cavitation numbers as follows: (A) 0.37, (C) 0.10, (D) 0.069, (G) 0.052, and (H) 0.044. The real and imaginary parts are denoted by the solid and dashed lines, respectively. The quasistatic resistance from the slope in Fig. 2 is indicated by the arrow.

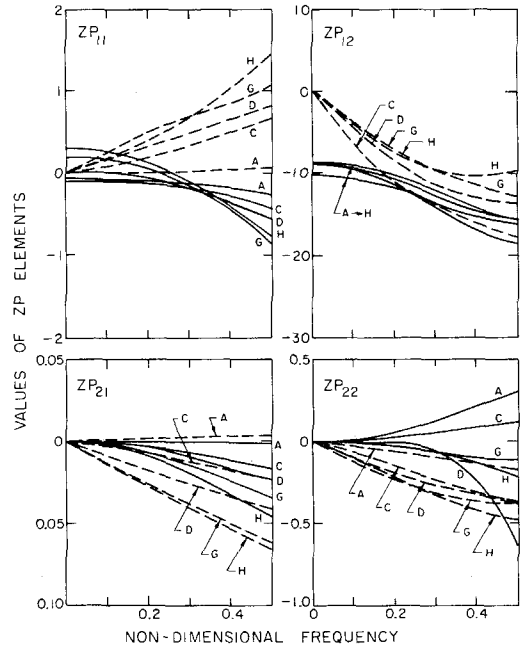

Fig. 5 Polynomial curve fits to the 10.2 cm impeller transfer matrices of Fig. 4

was little cavitation, down to $\sigma = 0.045$ for the pont H at which there was extensive cavitation and the impeller was on the verge of breakdown. For purposes of clarification and comparison with similar graph for the 7.6 cm impellers (Brennen [2]), polynomial fits were made to these data of the form

$$ZP_{IJ} = \sum_{N=0}^{N_{IJ}} a_{NIJ} (j\omega)^N \tag{1}$$

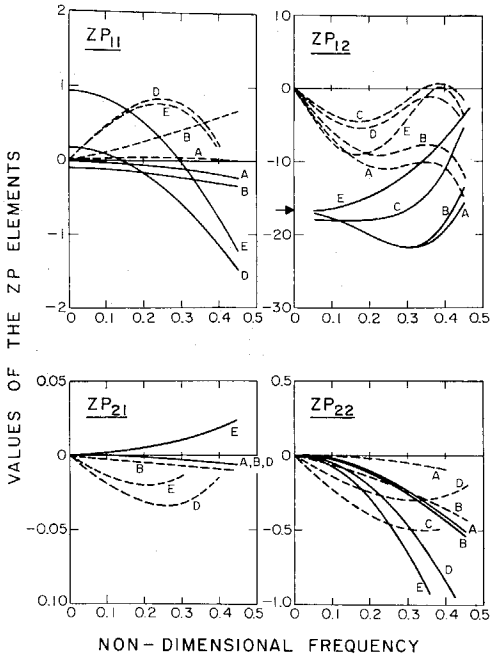

Fig. 6 Polynomial curve fits to the 7.6 cm impeller transfer matrices obtained at ϕ = 0.07 and a rotating speed of 9000 rpm by Ng and Brennen [1]. The cavitation numbers are (A) 0.51, (B) 0.11, (C) 0.046, (D) 0.040, and (E) 0.023. The quasistatic resistance from the slope in Fig. 2 is indicated by the arrow. (Reproduced from reference [2]).

where $N_{11} = N_{21} = N_{22} = 3$, $N_{12} = 5$, and a_{021} and a_{022} were set to zero in order to satisfy quasistatic continuity of mass [9]. Some of the resulting smoothed transfer functions are presented in Fig. 5. The comparable figure for the 7.6 cm impellers was included in reference [2] and is reproduced here as Fig. 6. In that figure the letters do not refer to the points in Fig. 3, but to those in Fig. 4 of reference [1].

The trends with cavitation number which were discussed in references [1] and [2] are similar for the two impellers. It is quite clear that in both cases a quasistatic model would only be appropriate for reduced frequencies less than about 0.1. Though a more detailed comparison will be included as part of the correlation with theory in Section 7, the following comments should be made on each of the ZP elements. Beginning with the impedance, ZP_{12}, it is clear from Figs. 5 and 6 that the trend of the resistance (or negative of the real part of ZP_{12}) correlates fairly well in both cases with the quasistatic resistance which can be obtained from the slope of the performance curves in Fig. 2. However these initial values differ in the two cases, not because of scale, but due to differences in pressure recovery in the volute as discussed in Section 2. Furthermore, it is apparent that under non-cavitating conditions the resistance in the 10.2 cm impeller increases more dramatically with frequency than in the 7.6 cm impeller. The reason for this is not clear but it may be a property of the flow at discharge and in the volute rather than a property of the inducer itself. Incrementally, cavitation causes a decrease in the resistance at higher frequencies although this is more marked with the 7.6 cm impeller. The inertial component of the impedance (negative of the imaginary part of ZP_{12}) is larger for the larger impeller. Cavitation causes incremental decreases in this component at higher frequencies which are similar for the two impellers.

Turning to the other three components, it should be stressed that in theory all of them should be zero for a completely rigid system, an incompressible fluid, and no cavitation. Apart from some unexplained discrepancies in ZP_{22}, this appears to be the case for both impellers. For example, nonzero values for ZP_{11} and ZP_{21} can be attributed entirely to the presence of cavitation. The comparison of Figs. 5 and 6 indicates good

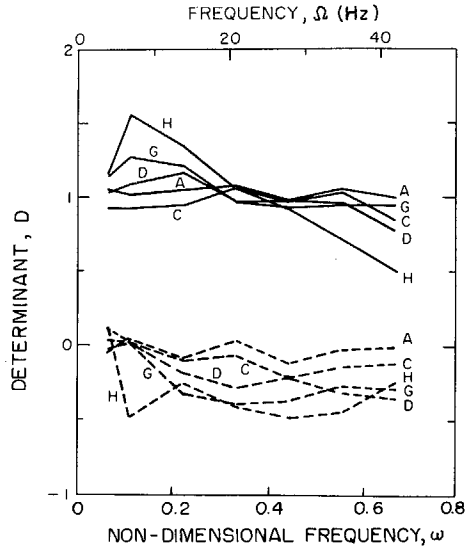

Fig. 7 The determinant, D, for the transfer matrices of Fig. 4. Real and imaginary parts are represented by the solid and dashed lines, respectively.

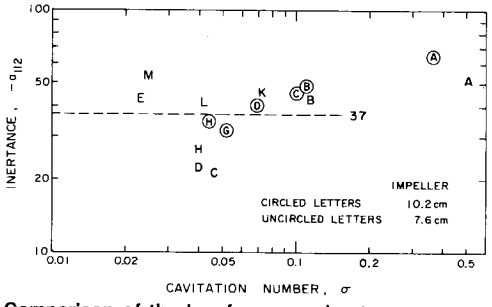

Fig. 8 Comparison of the low frequency inertances, $-a_{112}$, for the two impellers and equaton (9)

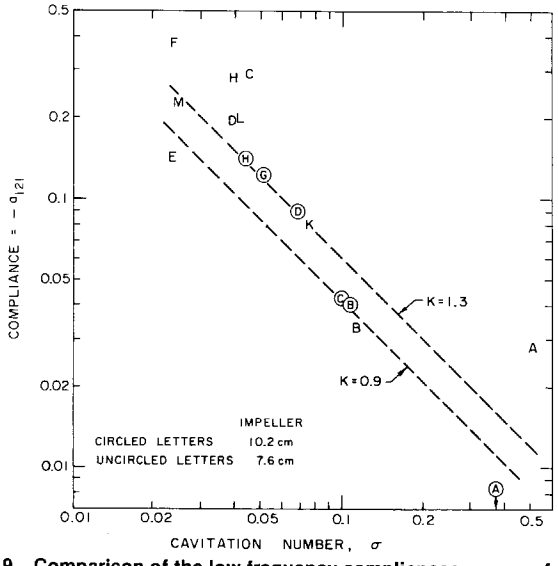

Fig. 9 Comparison of the low frequency compliances, $-a_{121}$, for the two impellers and equation (10) with K = 1.3 and 0.9

agreement between the two impellers insofar as the pressure gain term (ZP_{11}) and its variation with cavitation number are concerned. The imaginary part of ZP_{21} which is generally termed the compliance increases with σ in the expected manner in both cases. However, the larger impeller yielded negative real parts for ZP_{21} which did not occur for the smaller impeller. Finally, the general character of the incremental changes with cavitation number in the mass flow gain term (ZP_{22}) are similar in both cases.

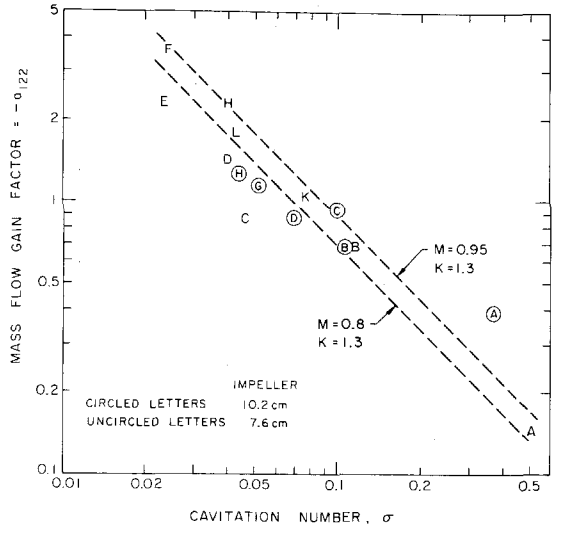

Fig. 10 Comparison of the low frequency mass flow gain factors, $-a_{122}$, for the two impellers and equation (11) with $K = 1.3$, $M = 0.8$, and 0.95

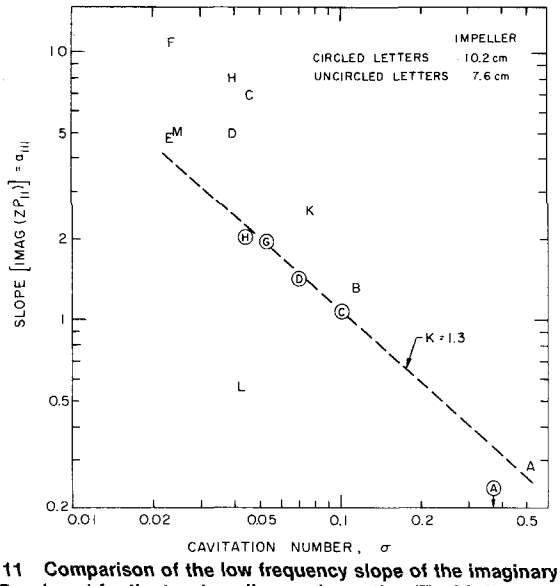

Fig. 11 Comparison of the low frequency slope of the imaginary part of ZP_{11}, (a_{111}) for the two impellers and equation (7) with $K = 1.3$, $F = 0$

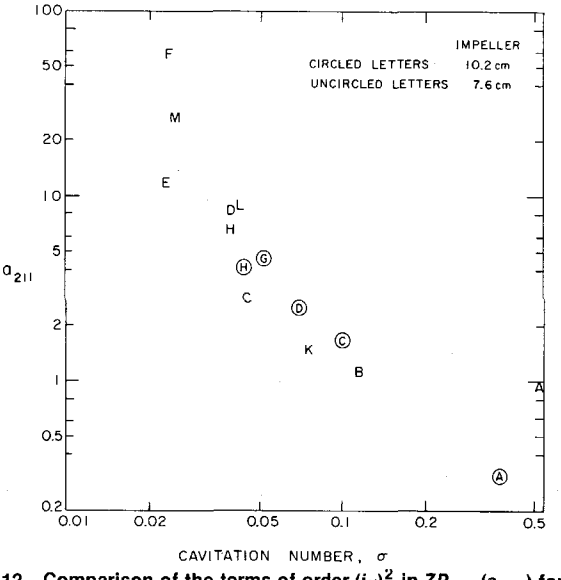

Fig. 12 Comparison of the terms of order $(j\omega)^2$ in ZP_{11}, (a_{211}) for the two impellers

The significance of the determinant, D, of $[ZP] + [I]$ has been discussed previously ([1], [2], [6]); the deviation from a value of unity presents some measure of the extent to which the dynamics of the pump have become potentially active. The determinants of the 10.2 cm impeller transfer matrices of Fig. 4 are plotted in Fig. 7. This exhibits the same features discussed previously for the 7.2 cm impeller [1]. Without cavitation the determinant is indeed unity; increasing the amount of cavitation results in progressive departure from passive dynamics. It has recently been demonstrated that serious system instabilities can result from this trend of increasingly active dynamics at lower cavitation numbers [6].

All of the above results were obtained close to the design flow coefficient, $\phi = 0.07$ and at an ambient temperature of 21°C. Some transfer functions were obtained at other flow coefficients (up to 0.076) and temperatures (up to 74°C) to investigate both off-design and thermodynamic effects. Only minor variations in the transfer functions were observed.

5 Comparison with the Bubbly Flow Model

The bubbly flow model yields theoretical transfer matrices given by equations (35) through (38) of reference [2]. They are functions of geometrical parameters, the flow coefficient, a blade-passage friction parameter, the mean length of the cavitating region (a surrogate cavitation number parameter) and, of course, the reduced frequency, ω. In addition, it is necessary to assume values for the two parameters K and M described in the Introduction. The purpose of this section will be to compare the model with experimental results described above. To begin with, however, it is instructive to confine attention to a comparison at the lower frequencies. The complicated expressions for the theoretical transfer matrices reduce at low frequencies to the following approximate relations:

$$ZP_{11} \simeq K\phi F\epsilon + j\omega K\tau\epsilon\{\cot\gamma + (1-\epsilon/2)F + \phi/\sin^2\gamma\} \quad (2)$$

$$ZP_{12} \simeq -2j\omega\tau/\sin^2\gamma - 2\cot\gamma - 2F \quad (3)$$

$$ZP_{21} \simeq -j\omega\epsilon\tau K/2 \quad (4)$$

$$ZP_{22} \simeq -j\omega\epsilon\tau\{M/\phi - K\phi/\sin^2\gamma\} \quad (5)$$

These expressions include only the terms of order $(j\omega)^0$ and $(j\omega)^1$ resulting from an expansion for small ω (the third order terms are long and involved and will not be repeated here). Correlation with the polynomial form (1) used to fit the data yields the following relations which must presumably hold if the model has value:

$$a_{011} = K\phi F\epsilon \quad (6)$$

$$a_{111} = K\tau\epsilon\{\cot\gamma + (1-\epsilon/2)F + \phi/\sin^2\gamma\} \quad (7)$$

$$a_{012} = -2\cot\gamma - 2F \quad (8)$$

$$a_{112} = -2\tau/\sin^2\gamma \quad (9)$$

$$a_{121} = K\tau\epsilon/2 \quad (10)$$

$$a_{122} = -\tau\epsilon\{M/\phi - K\phi/\sin^2\gamma\} \quad (11)$$

With these expressions, a three-way comparison will be made between the values for the a_{NIJ} coefficients derived from the experiments on 7.6 cm and 10.2 cm impellers and the values calculated from the expressions (7)-(11). For this purpose note that the impellers have a blade angle at the tip of $\gamma = 9°$ and a geometric value of τ of 0.45.

The simplest component to start with is the inertance, $-a_{112}$, which is plotted against cavitation number in Fig. 8. From equation (9) the theoretical first order term with $\tau = 0.45$ yields a value of 37. It can be seen from the experimental data that the actual inertance first decreases somewhat as the cavitation number is lowered and then increases at lower

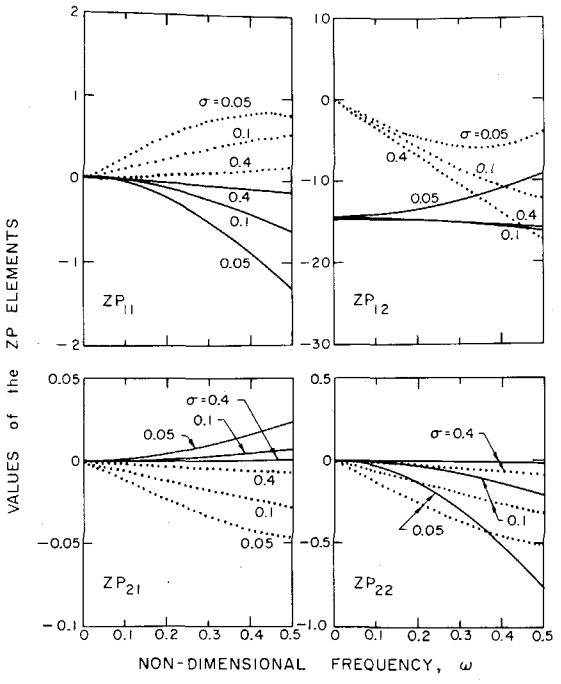

Fig. 13 Transfer functions calculated from the complete bubbly flow model with $\phi = 0.07$, $\gamma = 9$ deg, $\tau = 0.45$, $F = 1.0$, $K = 1.3$, and $M = 0.8$. Various cavitation numbers according to $\epsilon = 0.02/\sigma$ are shown.

cavitation numbers. Although the first order term in the theory is a simple constant, the complete expressions indicate similar theoretical trends with cavitation number (see reference [2] and Fig. 13). Note that the two impellers yield similar results. However, the value of 37 is probably low due to the neglect of the fact that the cross-sectional area of the flow is decreasing through the impeller as the hub radius increases; this would yield higher values for the inertance or a higher equivalent value of τ of about 0.6.

The observed experimental relation [2] between σ and $\epsilon = 0.02/\sigma$, permits comparison of the compliance, $-a_{121}$, and mass flow gain factor, $-a_{122}$, which are presented in Figs. 9 and 10. Both figures indicate consistency between the two sets of experimental results even though the older data for the 7.6 cm impeller is more scattered. They are also consistent with the trend exhibited by the theoretical expressions (10) and (11); it would appear that K and M values of about 1.3 and 0.8, respectively, best fit the data.

The slope of the imaginary part of ZP_{11}, (a_{111}) is presented in Fig. 11; the term involving F in the relation (7) has been omitted for this purpose and, not unexpectedly, the resulting theoretical line in Fig. 11 is on the lower side of the experiments. The magnitude of the zeroth order real part of ZP_{11}, (a_{011}) is small, positive, and increases with decreasing σ in both theory and experiment. In practice, however, the real part of ZP_{11} is dominated by terms of order $(j\omega)^2$ and higher as can be seen in Figs. 5 and 6. It is therefore more useful to present plots of the experimental values of a_{211} as has been done in Fig. 12. Here again the results of the experiments for the two impellers are similar.

Finally, the complete bubbly flow model has been used with $\gamma = 9$ deg, $\tau = 0.45$, $\phi = 0.07$, $F = 1$, $K = 1.3$, and $M = 0.8$, to produce the complete transfer function depicted in Fig. 13 for purposes of direct comparison with Figs. 5 and 6.

The value of F is unimportant and could just as well be set equal to zero; resulting changes in the transfer matrices are minor, the most obvious being an increase in the $\omega \to 0$ intercept of $\mathrm{Re}(ZP_{11})$ as F is increased.

Comparison with Figs. 5 and 6 reveals quite similar qualitative trends in virtually all of the elements of the transfer matrices. The most notable exception is the $\mathrm{Re}(ZP_{21})$; this component, however, is usually rather unimportant in determining the stability of a hydraulic system (reference [6]).

6 Conclusions

Dynamic transfer functions for two geometrically similar impellers, 7.6 and 10.2 cm, have been obtained compared, and analyzed. Within the data scatter there is little evidence of any effect of size or speed apart from that implicit in the nondimensionalization of total pressures, mass flow rate, and frequencies. The quality of the 10.2 cm impeller data is better than the previous data for the 7.6 cm impeller because of improved flow rate measurements using the EM meters.

The data for both impellers has also been compared with the predictions of the bubbly flow model (reference [2]). This comparison documents values of 1.3 and 0.8 for the two unknown constants (K and M) implicit in the model. It then appears that the bubbly flow model has considerable merit and yields theoretical transfer matrices within the experimental uncertainty.

Acknowledgments

The authors are grateful for the help of A. J. Acosta, D. Braisted, G. Hendrikson, and C. Park. The support of the NASA George Marshall Space Flight Center, Huntsville, Alabama, under Contract No. NAS 8-29313 and the National Science Foundation under Grant Eng. 76-11225 is also gratefully acknowledged.

Statement of Uncertainties Not Given in Figure Captions

Uncertainties in the measured transfer functions presented in Fig. 4 were evaluated using methods described in reference [1]. Ordinate error bars based on both (i) the influence of individual measurement scatter, and (ii) the influence of individual excitation modes on the resulting transfer functions, were evaluated for each point plotted in the figure. The results were similar to those presented in reference [1]. The uncertainty in the polynomial fitted transfer functions of Figs. 5 and 6 is evident from the comparison with data from which they were derived. The possible scatter in Fig. 7 is a direct result of the possible error in Fig. 4, and is ± 0.05 at most. The ordinate scatter in Figs. 8, 9, 10, 11, and 12 is self evident.

References

1 Ng, S. L., and Brennen, C., "Experiments on the Dynamic Behavior of Cavitating Pumps," ASME JOURNAL OF FLUIDS ENGINEERING, Vol. 100, 1978, pp. 166–176.

2 Brennen, C., "Bubbly Flow Model for the Dynamic Characteristics of Cavitating Pumps," *Journal of Fluid Mechanics*, Vol. 89, Part 2, 1978, pp. 223–240.

3 Shercliff, J. A., *The Theory of Electromagnetic Flow Measurement*, Cambridge University Press, 1962.

4 Rocketdyne Report, "Test Results of SSME Low Pressure Oxidizer Turbopump Model Inducer," Internal Letter No. R/H 4194-3074, 1974.

5 Brennen, C., "On Noncavitating Axial Inducer Performance," A brief unpublished note, 1977.

6 Braisted, D., "Cavitation Induced Instabilities Associated with Turbomachines," Ph.D. thesis, California Institute of Technology, Pasadena, Calif., 1979.

7 Ghahremani, F. G., "Turbopump Cavitation Compliance," Report No. TOR-0059 (6531-01)-2, Aerospace Corp., El Segundo, Calif., 1970.

8 Vaage, R. D., Fidler, L. E., and Zehnle, R. A., "Investigaton of *Characteristics of Feed System Instabilities*," *Final Report MCR-72-107*, Martin Marietta Corp., Denver, Col., 1972.

9 Brennen, C. and Acosta, A. J., "The Dynamic Transfer Function for a Cavitating Inducer," ASME JOURNAL OF FLUIDS ENGINEERING, Vol. 98, 1976, pp. 182–191.

10 Brennen, C., "The Dynamic Behavior and Compliance of a Stream of Cavitating Bubbles," ASME JOURNAL OF FLUIDS ENGINEERING, Vol. 95, 1973, pp. 553–542.

11 Brennen, C. E., Meissner, C., Lo, E. Y., and Hoffman, G. S., "Scale Effects in the Dynamic Transfer Functions for Cavitating Inducers," ASME Paper 80-WA/HT-51, Nov. 1980.